A HYBRID MODEL FOR INTERFEROMETRIC AND POLARIMETRIC P-BAND SAR IMAGING OF FORESTS

Maciej J. Soja[1] **and Lars M. H. Ulander**[2]

[1]*Chalmers University of Technology, SE-412 96 Göteborg, Sweden*
[2]*Swedish Defence Research Agency, SE-581 11 Linköping, Sweden*

ABSTRACT

In this paper, a forward model for extended covariance matrix prediction for boreal and hemi-boreal forest in P-band SAR is presented. The main product is the extended covariance matrix scaled to sigma nought on the diagonal. The input parameters consist of basic radar setup, topography, forest biome, biomass, and some model parameters. Backscatter intensities for HH, VV, and HV channels are predicted from biomass using regression based on BioSAR 2007 campaign data. The phase of the correlation between the HH and VV channels is found to be proportional to biomass and is also modelled by a regression based on BioSAR 2007 data. The coherence of HH and VV channels is found to be unrelated to biomass and is chosen to be modelled as a stochastic variable. The correlation of any co-polarized channel with HV is set to 0. The interferometric correlation values for the three channels are modelled using volume over ground (VoG) model, which is a combination of random volume over ground (RVoG), oriented volume over ground (OVoG), and elevated random volume over ground (ERVoG) models.

The forward model is also evaluated against SAR data from the BioSAR 2007 campaign. Three intensity images and one complex polarimetric correlation image are created for Remningstorp (site of BioSAR 2007) from existing biomass map, DEM, and flight path information. These images are compared with the images acquired with ESAR during the BioSAR 2007 campaign and the similarities and differences are discussed. The presented forward model is able to predict backscatter with an RMSE of 1.35 dB (HV), 1.77 dB (VV), and 1.92 dB (HH). Polarimetric correlation can be predicted with magnitude and phase RMSE equal to 0.08 and 16.3 deg, respectively. A qualitative evaluation of the interferometric part is also done and it is concluded that a good setup of model parameters is neccessary to get satisfactory results.

1. INTRODUCTION

In view of the proposed ESA Earth Explorer BIOMASS mission, a polarimetric interferometric forward model for P-band forest imaging is developed. The model predicts the 6x6 extended covariance matrix C_6 and requires only a limited number of input variables such as: relevant biophysical parameters (forest biomass and/or forest height, forest type, surface slopes), instrument parameters (incident angle, etc), and mission parameters (such as temporal and spatial baselines). The model simulates all the mechanisms that are exploited by the different biomass retrieval methods (intensity-based retrieval, PolInSAR height inversion, and polarimetric decomposition-based biomass retrieval).

Three BioSAR campaigns have been carried out as parts of the BIOMASS project: BioSAR 2007 (Hajnsek et al. 2008; Sandberg et al. 2009), BioSAR 2008 (Hajnsek et al. 2009; Soja et al. 2010), and the most recent BioSAR 2010 (at the time of writing, processed SAR data are not yet available). The main goal of these campaigns is to examine issues such as seasonal change and topography variation influence on SAR data in boreal and hemi-boreal forests of Sweden.

This text is structured in the following way: first, a short presentation of the experimental data used in this study is given in Sec. 2. In Sec. 3, the forward model is presented. First, the required product and the specified input variables are defined, and then each separate part of the forward model is described. In Sec. 4, the model is put into work and some sample results are presented, compared with ESAR data, and evaluated. Finally, Sec. 5 evaluates the whole study and pinpoints the most important observations. This text describes the latest implementation of the model. Some features, such as temporal decorrelation, different biome types, and different profile functions, will be described in the text, but not evaluated due to the limited character of this paper. Nevertheless, they will be available for the final delivery of the model. The model is suitable for extended covariance matrix prediction for boreal and hemi-boreal forests with standwise biomass range 0-300 tons/ha with an approximate resolution cell size of 0.5 ha.

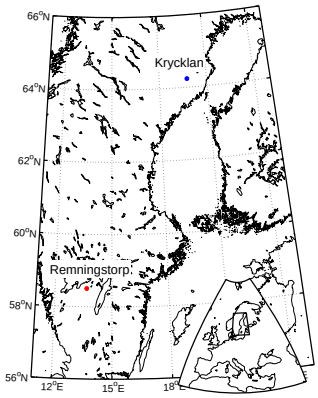

Figure 1. The two test sites in Sweden used for the three BioSAR campaigns.

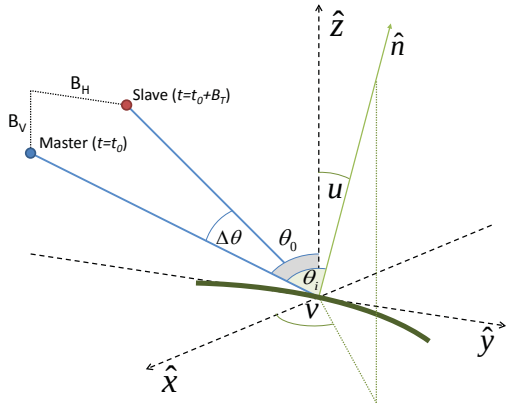

Figure 2. The geometry and nomenclature used throughout this paper. $\vec{n}$ is the normal of the ground surface.

2. EXPERIMENTAL DATA

In this study, P-band SAR data and ground truth data from Remningstorp in southern Sweden is used. A short description of the used data will be given below. A detailed description of the BioSAR 2007 campaign can be found in Hajnsek et al. (2008); Sandberg et al. (2009). Limited stand-wise forest data from Krycklan in Sweden is also used.

2.1. Test Site

Remningstorp is located in southern Sweden (58°30'N, 13°40'E, see Fig. 1) and covers about 1200 ha of productive forest land. The forest is classified as hemi-boreal. The dominant tree species are Norway spruce, Scots pine, and birch. The dominant soil type is till with a field layer consisting of different herbs, blueberry and narrow thinned grass. In denser old spruce stands the field layer is absent. The ground elevation is moderately varying between 120 and 145 m above sea level.

2.2. Field and Laser Scanning Data

There are two sets of field data available for Remningstorp. The first set consists of 10 stands, each of size 80x80 m^2, where every single tree with a diameter at breast height larger than 5 cm was recorded between 2007 and 2008. Stem diameter together with tree species, stem tilt and tree position were also recorded. About 10% of the trees in each stand had also their height measured. The stand biomass was estimated from stem diameter and tree height measurements using suitable allometric formulas with high accuracy.

The second set of Remningstorp ground truth data consists of 58 stands with areas between 0.5 and 9.4 ha. A stem volume map for Remningstorp was created from high-resolution canopy elevation models acquired with lidar scanning. Highly accurate biomass estimates for the 58 stands were computed from the stem volume map with the aid of optical classification of species and well-established conversion factors. A little less accurate biomass map for Remningstorp was also created from the stem volume map using one single conversion factor (see Fig. 7). This map was used as input for the model, see Sec. 4.

2.3. SAR Data

Fully polarimetric and interferometric P-band SAR images of Remningstorp were acquired using DLR's Experimental SAR (ESAR) platform at three dates in 2007: March 9th, March 31st to April 2nd, and May 2nd. For simplicity, the three data sets will be called March, April, and May data, respectively. For each date, geocoded images from two headings: $179°$ (1 image) and $200°$ (2 images) were created. In this paper, only the 200-degree heading is used since it is the only one to cover all available stands. Also, a set of polarimetric-interferometric images in slant range geometry were acquired for the $200°$-heading at horizontal spatial baselines between 10 and 80 meters and temporal baselines of approximately 0, 1, or 2 months.

3. FORWARD MODEL

3.1. Extended Covariance Matrix

The quantity to be modelled by this forward model is the extended covariance matrix called C_6. Having two scattering vectors (for two geometries, or "master" and "slave" images, as shown in Fig. 2) as in Eq. (1) and Eq.

Table 1. Input variables to the forward model.

Var.:	Description [unit]:
General setup	
TRS	training data set used
Radar system setup	
ν_c	centre frequency [Hz]
H	altitude [m]
θ_0	global angle of incidence [deg]
B_H	horizontal baseline [m]
B_V	vertical baseline [m]
B_T	temporal baseline [days]
Ground topography	
h_0	ground height [m]
u	ground slope [deg]
v	slope direction [deg]
Forest parameters	
h_{100}	forest height (optional) [m]
h_c	canopy elevation [% of h_{100}]
$\mathcal{B}$	forest biomass [tons/ha]
RVoG model parameters	
FID	profile type (1: exponential, 2: Gaussian)
$\mu_{\rm HH}$	ground-to-volume ratio for HH
$\mu_{\rm VV}$	ground-to-volume ratio for VV
$\mu_{\rm HV}$	ground-to-volume ratio for HV
Exponential profile setup	
$\alpha_{\rm HH}$	extinction on top of the layer for HH [dB/m]
$\alpha_{\rm VV}$	extinction on top of the layer for VV [dB/m]
β	extinction change with height [dB/m^2]
Gaussian profile setup	
δ	scattering center mean elevation [% of h_{100}]
χ	scattering center standard deviation [% of h_{100}]
Temporal decorrelation setup	
τ_v	time constant for temporal decorrelation of volume [days]
τ_s	time constant for temporal decorrelation of surface [days]

(2):

$$\vec{k}_1 = [S_{1,\rm HH} \;\; S_{1,\rm VV} \;\; S_{1,\rm HV}]^T, \quad (1)$$

$$\vec{k}_2 = [S_{2,\rm HV} \;\; S_{2,\rm VV} \;\; S_{2,\rm HV}]^T, \quad (2)$$

where $S_{i,\rm PQ}$ is the complex scattering amplitude for image i and polarisation mode PQ, and ^{T} is the transpose operator, C_6 can be acquired by creating outer product combinations of these two as shown in Eq. (3):

$$C_6 = 4\pi \begin{bmatrix} \langle \vec{k}_1 \cdot \vec{k}_1^H \rangle & \langle \vec{k}_1 \cdot \vec{k}_2^H \rangle \\ \langle \vec{k}_2 \cdot \vec{k}_1^H \rangle & \langle \vec{k}_2 \cdot \vec{k}_2^H \rangle \end{bmatrix} = 4\pi \begin{bmatrix} T_{11} & \Omega_{12} \\ \Omega_{12}^H & T_{22} \end{bmatrix}, \quad (3)$$

where C_6 has been scaled to give σ^0 on diagonal and ^{H} is the Hermitian transpose (the transpose of the complex conjugate). Using the fact that the covariance of any co-polarised channel with the cross-polarised channel is (ideally) zero, polarimetric and interferometric elements of C_6 can now be re-written as shown in Eq. (4) and Eq. (5):

$$T_{ii} = \begin{bmatrix} \sigma^0_{i,\rm HH} & \rho_i \cdot A_i & 0 \\ \rho_i^* \cdot A_i & \sigma^0_{i,\rm VV} & 0 \\ 0 & 0 & \sigma^0_{i,\rm HV} \end{bmatrix} \quad (4)$$

which is a Hermitian matrix, and

$$\Omega_{12} = \begin{bmatrix} \widetilde{\gamma}_{\rm HH} \cdot B_{\rm HH} & \omega_{12} \cdot C & 0 \\ \omega_{21} \cdot C & \widetilde{\gamma}_{\rm VV} \cdot B_{\rm VV} & 0 \\ 0 & 0 & \widetilde{\gamma}_{\rm HV} \cdot B_{\rm HV} \end{bmatrix}, \quad (5)$$

which is non-Hermitian and where $i = 1, 2$ is the index of the studied image ("master" or "slave" in Fig. 2). The diagonal elements of T_{ii} are scaled to sigma nought:

$$\sigma^0_{i,\rm PQ} = 4\pi \left\langle |S_{i,\rm PQ}|^2 \right\rangle,$$

and they also give the following elements in Eq. (4) and Eq. (5):

$$A_i = \sqrt{\sigma^0_{i,\rm VV} \cdot \sigma^0_{i,\rm HH}},$$

$$B_{\rm PQ} = \sqrt{\sigma^0_{1,\rm PQ} \cdot \sigma^0_{2,\rm PQ}},$$

$$C = \sqrt{\sigma^0_{1,\rm HH} \cdot \sigma^0_{2,\rm VV}}.$$

Two complex valued quantities that need to be modelled are:

$$\rho_i = \frac{\langle S_{i,\rm HH} \cdot {S_{i,\rm VV}}^* \rangle}{\sqrt{\left\langle |S_{i,\rm HH}|^2 \right\rangle \left\langle |S_{i,\rm VV}|^2 \right\rangle}}, \quad (6)$$

$$\widetilde{\gamma}_{\rm PQ} = \frac{\langle S_{1,\rm PQ} \cdot {S_{2,\rm PQ}}^* \rangle}{\sqrt{\left\langle |S_{1,\rm PQ}|^2 \right\rangle \left\langle |S_{2,\rm PQ}|^2 \right\rangle}}, \quad (7)$$

which represent the polarimetric complex correlation and the interferometric complex correlation, respectively. Note, that $\widetilde{\gamma}_{\rm PQ}$ is the correlation of two interferometric images acquired in the same polarimetric mode. The symbolism has been minimised for simplicity.

The non-diagonal elements in Eq. (5), ω_{12} and ω_{21}, represent the correlation between HH and VV channels at both ends of the baseline. In this model, they will not be predicted using dedicated functions, but their values will be derived from the expressions for ρ_i and $\widetilde{\gamma}_{\rm PQ}$. The details will be presented in Sec. 3.6.

3.2. Input Parameters

The parameters which have been chosen to be required from the user are all shown in Tab. 1. Some of the parameters, together with the geometry of the problem, are visually presented in Fig. 2. The forest height indicator used in this text will be the h_{100}-parameter, which is defined as the mean height of the 100 tallest trees per hectare.

3.3. Backscatter Intensity Modelling

Backscatter intensity is chosen to be modelled by the following function:

$$[\widehat{\sigma^0_{\mathrm{PQ}}}]_{dB} = a_{\mathrm{PQ}} + b_{\mathrm{PQ}} \log_{10} \mathcal{B} + \epsilon_{\mathrm{PQ}}, \qquad (8)$$

where PQ is either HH, VV, or HV, and ϵ_{PQ} is a normally distributed additive error with mean 0 and standard deviation ς_{PQ}. In order to obtain suitable parameter values in (8), the functions were fitted to the 200-degree heading BioSAR data in the following constellations:

- $\mathsf{TRS} = 0$: all available data,
- $\mathsf{TRS} = 1$: March data only,
- $\mathsf{TRS} = 2$: April data only,
- $\mathsf{TRS} = 3$: May data only.

The resulting parameter values are presented in Tab. 2. In Fig. 3, the fitted lines are plotted together with the corresponding training data. The same model with the same error representation is used for both "master" and "slave" images.

3.4. Polarimetric Correlation Modelling

The cross-channel complex correlation ρ_i is modelled by the following functions derived from empirical observations in BioSAR 2007 data:

$$|\widehat{\rho_i}| = \overline{\rho} + \epsilon_\rho, , \qquad (9)$$

$$\arg(\widehat{\rho_i}) = a_\rho + b_\rho \cdot \mathcal{B} + \epsilon_{\psi_\rho}, \qquad (10)$$

where $\overline{\rho}$ is the mean value of the cross-channel coherence and the phase changes linearily with biomass $\mathcal{B}$. Both the magnitude and the phase of ρ_i are distorted by zero mean additive errors ϵ_ρ and ϵ_{ψ_ρ} with standard deviations ς_ρ and ς_{ψ_ρ}, respectively.

The model presented in (9) and (10) was derived from observations in BioSAR 2007 data. The model was fitted to the data in the same way as described in Sec. 3.3. In Fig. 4 the resulting curves are plotted together with the original data points. Values of the constant parameters in (9) and (10) can be found in Tab. 2. The same model with the same error representation is used for both "master" and "slave" images.

3.5. Interferometric Correlation Modelling

The interferometric contributions $\widetilde{\gamma}_{\mathrm{PQ}}$ (meaning the complex correlation values of two images with the same polarization mode but different geometries and/or acquisition times) are predicted by a combination of the classical random volume over ground model (RVoG, see Papathanassiou & Cloude (2001); Cloude & Papathanassiou (1998, 2003); Cloude (2010)), the elevated random volume over ground model (ERVoG), and the oriented volume over ground model (OVoG), both in the form presented in Garestier et al. (2008), with all the profile functions described in Garestier & Le Toan (2010). The model presented here will be simply called volume over ground model (VoG), as it includes elements of all the three established models.

The RVoG model predicts the complex correlation of a random volume of particles (of height h_V) situated directly above a coherently scattering ground. In ERVoG, the volume is allowed to have an elevation h_c above the ground, thus imitating a tree crown of thickness $h_V - h_c$. The OVoG model allows the particles inside the volume to have a predetermined orientation, thus allowing the attenuation to be polarization-dependent.

The VoG model presented here also includes exponential functions simulating the temporal decorrelation of volume and surface in a very much simplified manner:

$$\widetilde{\gamma}_{\mathrm{PQ}} = \mathrm{e}^{ik_z h_0} \cdot \frac{\widetilde{\gamma}_{v,\mathrm{PQ}} \cdot \mathrm{e}^{ik_z h_c} \cdot \mathrm{e}^{-\frac{B_T}{\tau_{vol}}} + \mu_{\mathrm{PQ}} \cdot \mathrm{e}^{-\frac{B_T}{\tau_s}}}{1 + \mu_{\mathrm{PQ}}}, \qquad (11)$$

where

$$k_z = \frac{4\pi \cdot \Delta\theta}{\lambda \sin\theta_i}$$

is the vertical wavenumber,

$$\widetilde{\gamma}_{v,\mathrm{PQ}} = \frac{\int_0^{h_V - h_c} f_{\mathsf{FID},\mathrm{PQ}}(z) \cdot \mathrm{e}^{ik_z z}\,\mathrm{d}z}{\int_0^{h_V - h_c} f_{\mathsf{FID},\mathrm{PQ}}(z)\,\mathrm{d}z} \qquad (12)$$

represents the correlation for a volume ("tree crown") of thickness $h_V - h_c$ and a profile described by $f_{\mathsf{FID}}(z)$, and the other quantities are as defined in Fig. 2 and Tab. 1. Two main profiles presented in Garestier & Le Toan (2010) are:

$$f_{1,\mathrm{PQ}}(z) = \exp\left(\frac{2\sigma_{\mathrm{PQ}}(z) \cdot z}{\cos\theta_i}\right) \qquad (13)$$

and

$$f_{2,\mathrm{PQ}}(z) = \exp\left(-\frac{(z-\delta)^2}{2\chi^2}\right), \qquad (14)$$

where the first one is an exponential profile with height-dependent extinction coefficient $\sigma(z)$, and the second one is a Gaussian curve with mean δ and standard deviation χ. In Garestier & Le Toan (2010) three different types of $\sigma(z)$ are discussed, which all can be summarized as:

$$\sigma_{\mathrm{PQ}}(z) = \alpha_{\mathrm{PQ}} + \beta z, \qquad (15)$$

where polarization dependence of the α-parameter has been introduced as an extension of RVoG to OVoG. Parameter α should be specified among the other input parameters for both HH and VV polarisations, and α_{HV} is then simply:

$$\alpha_{\mathrm{HV}} = \frac{\alpha_{\mathrm{HH}} + \alpha_{\mathrm{VV}}}{2}. \qquad (16)$$

If $\beta = 0$, $\alpha_{\mathrm{HH}} = \alpha_{\mathrm{VV}}$, and $h_c = 0$, the classical RVoG model is used. The standard OVoG model can be obtained when $\beta = 0$ and $h_c = 0$. Likewise, the ERVoG

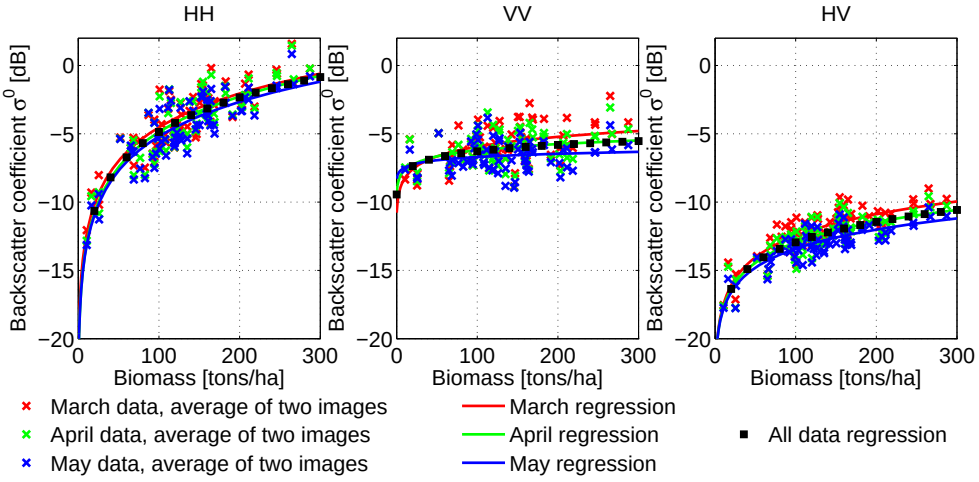

Figure 3. The model presented in (8) *was fitted to BioSAR data for each date separately, and for all dates together. The curves and data points are presented here.*

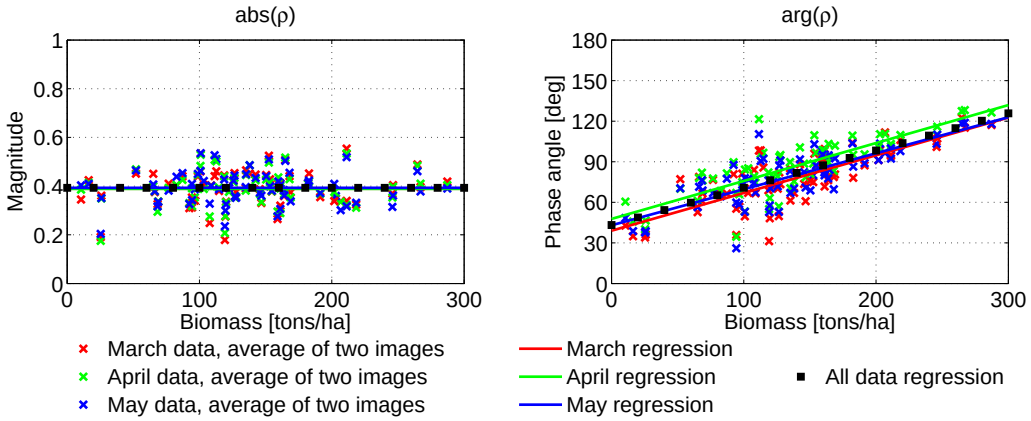

Figure 4. The model presented in (9) *and* (10) *was fitted to BioSAR 2007 data for each date separately and for all dates together. The fitted lines are presented here.*

model is obtained if $\beta = 0$, $h_c > 0$, and $\alpha_{\mathrm{HH}} = \alpha_{\mathrm{VV}}$. The integrals in Eq. (12) can be computed analytically (see Garestier & Le Toan (2010)).

The choice of the parameters h_c, B_T, τ_v, τ_s, and μ_{PQ}, together with the choice between one of the two profiles $f_1(z)$ and $f_2(z)$ (with the parameters α_{PQ} and β, or δ and χ therein) are all left to the user. Also, it is here assumed that

$$h_V \approx h_{100} \tag{17}$$

which has been shown to be quite a reliable approach (see for instance Hajnsek et al. (2008, 2009), where RVoG inversion gives h_V as a good estimate of h_{100}).

3.6. Non-diagonal Elements of Ω_{12}

The non-diagonal elements Ω_{12} will be modelled using the assumption that the combined decorrelation due to different polarizations *and* different acquisition points/time can be seen as a product of the polarimetric decorrelation and the interferometric decorrelation, that is:

$$\frac{\langle S_{i,\mathrm{PP}} \cdot {S_{j,\mathrm{QQ}}}^* \rangle}{\sqrt{\langle |S_{i,\mathrm{PP}}|^2 \rangle \langle |S_{j,\mathrm{QQ}}|^2 \rangle}} \approx \gamma_{pol} \cdot \gamma_{int} \tag{18}$$

which gives:

$$\omega_{12} \approx \gamma_{\mathrm{HH}} \cdot \rho_2 \approx \gamma_{\mathrm{VV}} \cdot \rho_1, \tag{19}$$

$$\omega_{21} \approx \gamma_{\mathrm{VV}} \cdot \rho_2^* \approx \gamma_{\mathrm{HH}} \cdot \rho_1^*, \tag{20}$$

where each ω has been re-written in two equivalent ways using the assumption in Eq. (18). In this forward model, the non-diagonal elements will be modelled in the following way:

$$\omega_{12} = \frac{\gamma_{\mathrm{HH}} \cdot \rho_2 + \gamma_{\mathrm{VV}} \cdot \rho_1}{2}, \tag{21}$$

$$\omega_{21} = \frac{\gamma_{\mathrm{HH}} \cdot \rho_1^* + \gamma_{\mathrm{VV}} \cdot \rho_2^*}{2}. \tag{22}$$

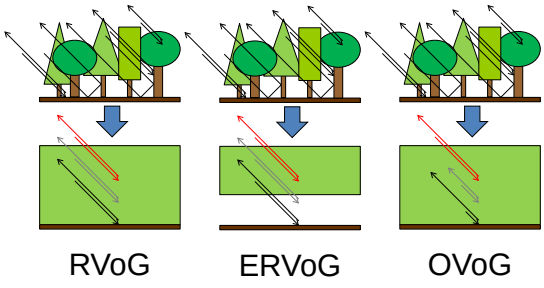

Figure 5. Random volume over ground model simulates complicated forest scattering as a combination of scattering from a random volume of height h_V and a coherently scattering surface. Coherence of different channels is simulated by taking volume and surface scattering in different proportions (different μ-values). Elevated random volume over ground (ERVoG) model allows the existence of a gap of width h_c between the volume and the ground. Oriented volume over ground (OVoG) introduces polarization-dependent attenuation in volume.

3.7. Biomass to Height Conversion

The volume over ground model requests the canopy height h_V as an input parameter. Since the assumption in Eq. (17) is used, h_{100} is going to be used as the volume height. Biomass and h_{100} can be related through the following allometric equation, which has been found valid for Remningstorp and Krycklan data:

$$\log_{10} h_{100} = a_h + b_h \log_{10} \mathcal{B} + \epsilon_h \qquad (23)$$

where a_h and b_h are parameters estimated using least-squares fitting to the available data, and ϵ_h is an additive error with zero mean and standard deviation ς_h. Using ground-measured values for h_{100} and $\mathcal{B}$ for Remningstorp and Krycklan (Hajnsek et al. 2009; Soja et al. 2010), these parameters can be estimated and a curve can be fitted, see Fig. 6. The estimated values for a_h, b_h and ς_h can be found in Tab. 2.

4. EVALUATION OF THE MODEL

The forward model described in this paper was evaluated using SAR data over Remningstorp acquired by the ESAR platform from DLR. One SAR image acquired in May at the 200-degree heading was used as reference. The previously mentioned lidar-based biomass map shown in Fig. 7 was inserted into the model. The ESAR images were down-sampled to fit the grid of the biomass map (pixel size: 10 m by 10 m). All presented maps are geo-coded to UTM33.

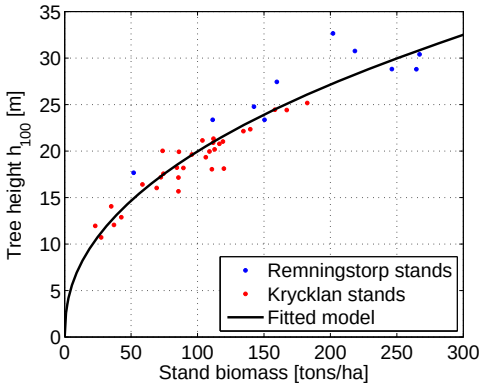

Figure 6. Allometric relation for biomass to height conversion. 10 stands in Remningstorp and 31 stands in Krycklan were used.

Table 2. Values of the parameters in models (8), (9), (10), *and* (23) *found by least-squares fitting to BioSAR data. ς_x is the standard deviation of the error ϵ_x (which has mean 0).*

	Training set used:			
Const.:	March	April	May	All
a_{HH}	-20.7625	-21.8742	-21.7738	-21.4701
b_{HH}	8.1223	8.5064	8.2956	8.3081
ς_{HH}	1.2599	1.3035	1.2748	1.3015
a_{VV}	-10.6582	-9.1717	-8.2603	-9.3634
b_{VV}	2.3590	1.4829	0.7784	1.5401
ς_{VV}	1.2843	1.1850	1.0778	1.2467
a_{HV}	-22.8652	-22.7809	-22.5807	-22.7423
b_{HV}	5.2002	4.9165	4.5876	4.9014
ς_{HV}	0.9088	0.8681	0.7472	0.9347
$\overline{\rho}$	0.3895	0.3886	0.3930	0.3904
ς_ρ	0.0714	0.0698	0.0669	0.0690
a_ρ	0.6815	0.8332	0.7509	0.7552
b_ρ	0.0049	0.0049	0.0046	0.0048
ς_{ψ_ρ}	0.2272	0.2137	0.2135	0.2272
a_h	N/A	N/A	N/A	0.4118
b_h	N/A	N/A	N/A	0.4441
ς_h	N/A	N/A	N/A	1.7213

4.1. Backscatter Intensity

The model was set to only use May data. In Fig. 8, the modelled SAR images are presented side-by-side with the original ESAR images. They are plotted as RGB images with HH as the red channel, VV as the green channel, and HV as the blue channel. Also, there are three bivariate (two-dimensional) histograms plotted to the right (one for each polarization).

The first, most obvious conclusion when comparing the two images is that the ESAR image shows many more small-scale effects such as border effects close to roads, forest boundaries, etc. This is an expected behaviour

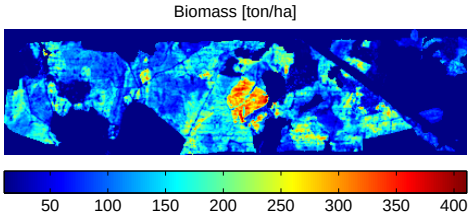

Figure 7. A laser scanning-derived biomass map with pixel size 10 m x 10 m was used as input to the forward model. The map has here been rotated 90° counterclockwise for space-saving reasons. Non-forested areas have been masked out.

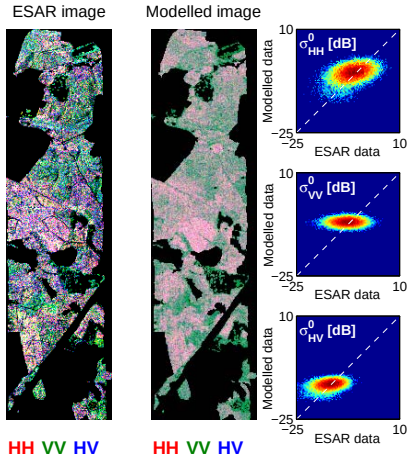

Figure 8. Simulation results for intensity modelling in Remningstorp.

since the model is developed for stand-wise data with stand areas above 0.5 ha. The resolution of the model can thus be approximated to 70 m x 70 m. Since the predicted images are on a grid of 10 m x 10 m, there are many effects unaccounted for. Nevertheless, the prediction of sigma nought backscatter shows good results on the bigger scale, see Fig. 8. Considering the fact that the conversion from stem volume map to biomass map was done in a rather simplified way using one constant only (independent of tree species), the results are certainly good on the stand level. The best prediction occurs for HV with a root-mean-square error of 1.35 dB, which has already been shown to give the best biomass correlation at P-band (Sandberg et al. 2009). HH gives higher error (1.92 dB) but still, both images show the same dynamic ranges. For VV, the knowledge of biomass is apparently not sufficient for satisfactory prediction of sigma nought — the dynamic range observed in ESAR data is far higher than the dynamic range of the model. Although the RMSE (1.77 dB) for VV is lower than for HH, there is no alignment of the data along the $y = x$-line.

Note: the presented RMSE errors were computed for modelled data based on biomass map *downsampled* to 70

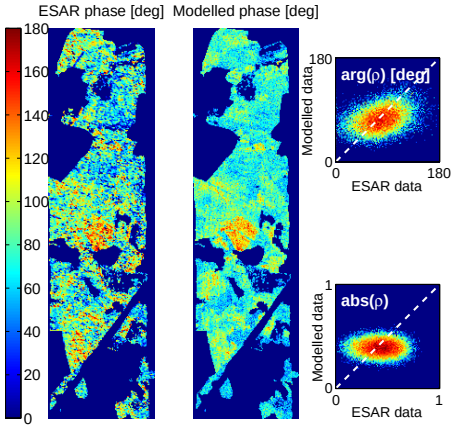

Figure 9. Simulation results for polarimetric correlation modelling.

m x 70 m pixels, which matches the smallest stand size in training data.

4.2. Polarimetric Correlation

In Fig. 9 the results for prediction of the HH-VV-correlation are shown. As it was earlier observed, the magnitude of ρ was not found to be biomass-dependent and thus only phase images are shown. There is a good correlation of the ESAR image and the image computed by the forward model. In the histogram for the phase of ρ, good results with no visible bias are observed. The statistics of both images are very much alike. When it comes to the magnitude of ρ, the ESAR image shows higher dynamic range than the predicted image. Even though the magnitude of ρ is seemingly uncorrelated with biomass, there may be some other factors that introduce the dynamic range. One other difference observed in the images is the "graininess" of the ESAR image. This is most likely caused by the effects of downsampling after multilooking in correlation computing, where a window of 17 pixels in azimuth and 9 pixels in range was used for that purpose. This even enhances the earlier mentioned issues connected to different resolutions of the forward model and the available biomass map. Nevertheless, the prediction of ρ_i can be done with an error of approximately 0.08 in magnitude and $16°$ in phase.

4.3. Interferometric Correlation

The interferometric part of the forward model was also tested against ESAR data. As the second ESAR image, an image from the same date, but with an approximate horizontal baseline of 70 m, was used. The exact flight path information was provided to the forward model in form of θ_0 and k_z maps. The other radar and forest parameters were chosen to resemble the ESAR case as well

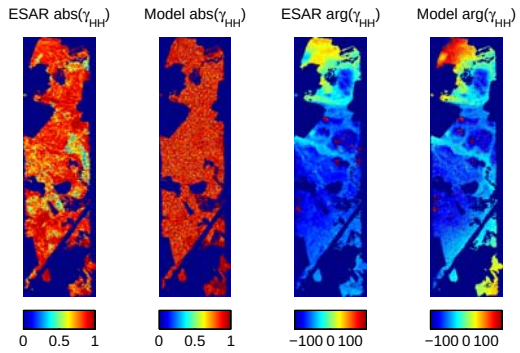

Figure 10. Correlation prediction results for HH.

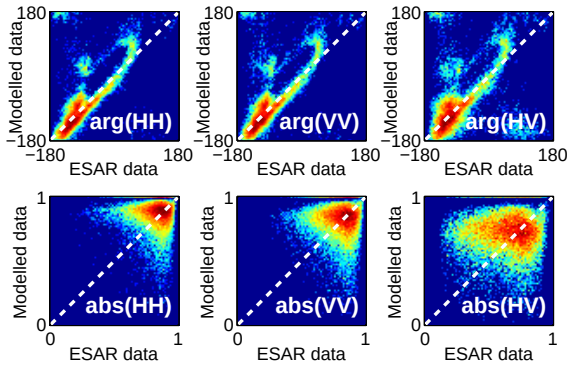

Figure 11. Correlation histograms.

as possible, based on information in Hajnsek et al. (2008). The height h_{100} was computed using Eq. (23). The unknown model parameters, mainly μ_{PQ} and the profile function with the parameters therein, were estimated using repetitive qualified guessing. In Fig. 10, an example of an interferometric correlation prediction is shown. In Fig. 11, histograms comparing modelled images with reference images for all three polarizations are shown. The phase resemblence is very good, mostly thanks to the detailed DEM provided to the model, but there are some issues in the regions corresponding to near and far range. The coherence values are in general well estimated, but the spread is big, and the spatial changes are not well reproduced. In the presented case, $h_c = 50\%$, $\mu_{\mathrm{HH}} = \mathcal{N}(10, 6^2)$, $\mu_{\mathrm{VV}} = \mathcal{N}(7, 4^2)$, $\mu_{\mathrm{HV}} = \mathcal{N}(4, 2^2)$, $\mathsf{FID} = 1$ and $\alpha_{\mathrm{HH}} = \alpha_{\mathrm{VV}} = 0.1$ dB/m. The fact, that the ground-to-volume ratios and the extinction coefficients are constant (or normally distributed), and not related to biomass must be one of the explanations to why the big scale changes are not reproduced. The next planned step to examine these model parameters and see if they can be related to biomass.

5. CONCLUSIONS AND FURTHER WORK

The evaluation of the proposed model shows, that the intensity and polarimetry parts can predict their corresponding quantities with good results. The interferometric part is based on a model that has shown itself to be functional, but the parameter settings still need some trimming.

An interesting observation is that the ground-to-volume ratios (μ_{PQ}) apparently need to be very high ($\mu \gg 1$) for all polarizations. As expected, HH shows highest penetration depth, which also results in higher coherence levels and higher ground-to-volume ratios. While at higher frequencies HV is often assumed to only consist of volume scattering, in P-band it shows high coherence not only due to quite large amount of ground scattering but also due to more stable scatterers in the volume (such as thicker branches).

This model does not simulate incident angle influence nor the influence of extreme ground topography. These effects need to be studied in future. Also, intensity and polarimetric correlation for master and slave images are not differentiated in the presented version of the model.

REFERENCES

Cloude, S. & Papathanassiou, K. 1998, IEEE Transactions on Geoscience and Remote Sensing, 36, 1551

Cloude, S. & Papathanassiou, K. 2003, IEE Proceedings on Radar, Sonar & Navigation, 150, 125

Cloude, S. R. 2010, Polarisation Applications in Remote Sensing (Oxford University Press)

Garestier, F., Dubois-Fernandez, P. C., & Champion, I. 2008, IEEE Transactions on Geoscience and Remote Sensing, 46, 3544

Garestier, F. & Le Toan, T. 2010, IEEE Transactions on Geoscience and Remote Sensing, 48, 1528

Hajnsek, I., Keller, R. S. M., Horn, R., et al. 2009, BioSAR 2008 Technical Assistance for the Development of Airborne SAR and Geophysical Measurements during the BioSAR 2008 Experiment: Draft Final Report - BioSAR Campaign, Tech. rep., European Space Agency, ESA contract no. 22052/08/NL/CT

Hajnsek, I., Scheiber, R., Ulander, L., et al. 2008, BioSAR 2007 Technical Assistance for the Development of Airborne SAR and Geophysical Measurements during the BioSAR 2007 Experiment: Final Report without Synthesis, Tech. rep., European Space Agency, ESA contract no. 20755/07/NL/CB

Papathanassiou, K. & Cloude, S. 2001, IEEE Transactions on Geoscience and Remote Sensing, 39, 2352

Sandberg, G., Ulander, L. M. H., Fransson, J. E. S., Holmgren, J., & Le Toan, T. 2009, Remote Sensing of the Environment, accepted for publication

Soja, M. J., Sandberg, G., & Ulander, L. M. H. 2010, in Proceedings of the 2010 IEEE International Geoscience and Remote Sensing Symposium